Bifurcation analysis of pressure-induced detachment of a rod adhered to a plate

S. S. Turzi [*1], D. Ambrosi [†2], and M. Zoppello [‡2]

[1]Dipartimento di Matematica, Politecnico di Milano, Piazza Leonardo da Vinci 32, 20133 Milano, Italy
[2]DISMA, Politecnico di Torino, Corso Duca Degli Abruzzi 24, 10129 Torino, Italy

September 6, 2024

Abstract

We study the lift of an elastica adhering to a flat rigid surface induced by a pressure difference. Adhesion is modelled by a cohesive force that decreases linearly with separation. Using a non-linear local analysis, we determine the bifurcation diagram that governs the peeling process under quasi-static conditions. We show that the delamination emerges through a discontinuous transition: a normal form of the bifurcation diagram allows us to draw in a simple way the main physical mechanism, elucidating the local validity of the theory at the transition. We predict that the pressure, as a function of the detachment length, undergoes an initial drop followed by an approximately constant behaviour, while the detachment length at the transition is always finite and is roughly proportional to the elasto-adhesion length. This analysis can be the starting point to understand more complex related problems which arise in fracture mechanics or in biology, such as testing of adhesives in a flowfield and the arterial dissection.

keywords: Rod, adhesion, delamination, mechanical instability, bifurcation, Lyapunov-Schmidt.

1 Introduction

Because of its common occurrence, the mechanics of peeling has been subject of much scientific interest and investigation [19]. The mechanics of adhesive contacts is relevant for a variety of practical applications, such as the design of adhesives and coatings, the fabrication of flexible electronics [15], the design of soft robots [3], the development of tough medical bandages[29, 30], the analysis of biological attachment devices [1].

From a mathematical and experimental perspective, adhesion phenomena constitute a challenging area of research. The physics underlying the adhesion crucially depends on the

[*]corresponding author: stefano.turzi@polimi.it
[†]davide.ambrosi@polito.it
[‡]marta.zoppello@polito.it

properties at the microscale level of the material, the adhesive properties of the surfaces of the bodies in contact. However, some relatively simple models are able to capture the essentials of the complex phenomena involved in adhesion. A common strategy is to assume a membrane-like behaviour for the elastic body and introduce an adhesion energy proportional to the measure of the detached zone [12, 13, 22, 6, 19]. Exploiting a simple energy balance argument, it is possible to derive the critical detachment conditions by comparing the energies involved (bending, stretching, potential energy of the external force or pressure, and adhesion), and derive, for example, the relationship between the magnitude of the constant force and the peel angle between the rod and the rigid surface.

The classical peeling model reads as an elastic rod adhering to a adhesive rigid flat surface: the rod is lifted by a constant force, applied on one boundary of the rod, directed orthogonally to the basement. Another common mechano-adesive system is the blister test [5, 27, 16]: an elastomeric membrane adhering to a rigid substrate with a hole is subject to a pressure difference across the non attached area, so that it forms a noticeable blister. For increasing pressure, the blister radius is first unchanged, until a threshold beyond which the crack rapidly increases in size and the stored strain is relaxed. In general, the pressure at this point in time is not the maximum pressure recorded during the experiment.

Irrespectively of the specific system at hand, the energy balance approach is simple and effective in describing the peeling mechanics, but it inherently lacks some physical information about the adhesion force. An alternative approach is to use a cohesive zonal model [21, 7, 28], i.e., to introduce a constitutive law for the adhesive force, limited to a thin cohesive layer close to the substrate. The equilibrium solutions are then obtained using force and momentum balances, which provide more information about adhesion process and the stresses involved.

Both for the classical peeling and for the blister problem, a rigorous nonlinear and analytical study of the unbonding transition is uncommon, even for the simplest cases where an analytical treatment is possible. This is largely due to the fact that even the simplest adhesion laws are non-smooth, typically piecewise linear, and therefore make both analytical and numerical study difficult. In this work, we propose a different approach to this type of problem. By making a linear extrapolation of the adhesion law in the region of interest, it is possible to analyse the problem as a classical bifurcation problem for which many advanced mathematical techniques are available. We show that it is not enough to study the linearized problem, but that it is necessary to proceed with a weakly nonlinear analysis in order to correctly interpret the nature of the delamination. This approach provides a very simple and intuitive representation of delamination, in terms of normal form and effective potential (equivalent to a Landau potential in the study of phase transitions) that other approaches do not have.

In particular, we focus on the problem of delamination by pressure: an elastic rod attached to a rigid surface is lifted by a constant pressure. This system can be seen as is an intermediate step in representing a rod lifted by a flowfield, like an adhesive tapes on an aircraft. It can be seen as a mixed problem between peeling and blister, preserving the challenges of both of them: the driving force is a pressure, but one boundary is free. This problem cannot solved by using a simple energy balance argument, since the rod has finite bending stiffness so that the shape of the rod, thus its bending energy, is part of the problem.

In this work we perform a mathematical analysis of the delamination problem. Our main aim is to identify the critical threshold in pressure and determine how the geometry of the detachment depends on the material parameters and applied forces. A relevant question is to determine whether the transition (the detachment) is continuous (second-

order) or discontinuous (first-order) versus pressure. It is useful to have an analytical description of the order of the transition because it is often difficult to assess the difference between a steep continuous and a discontinuous transition by means of experiments, numerical simulations, or even closed-form equilibrium solutions. First and second-order transitions are subject to fundamentally different physical mechanisms: while a continuous transition is essentially reversible, meaning that it retraces the same family of solutions if the control parameter is inverted, in a first-order transition it is possible to observe hysteresis phenomena where the solution traces a different branch of the solution and it is therefore not possible to return the system to its initial state simply by reversing the process. Finally, an analytical study also provides a mathematical representation of the transition in terms of a normal form and an effective potential. This can also foster a deeper intuitive understanding of the phenomenon.

Motivated by the aforementioned objectives, we perform a non-linear analysis of the bifurcations occurring in the delamination problem: using a cohesive zonal model we show how the bifurcated branches depend on the material features of the cohesive forces (magnitude and slope versus the vertical displacement). We prescribe an adhesive phenomenological constitutive law: adhesion forces act in a cohesive zone of finite thickness. To model degradation, the force is assumed to be a linear decreasing functions of the separation distance [21, 7, 26, 25].

The outline of this paper is as follows. In §2, the relevant background notions on adhesion and the elastic rod theory are introduced, and in Appendix A we perform the variational derivation of the equilibrium equations for the problem of an elastica in contact with a sticky rigid surface. Particular attention is also placed on compatibility conditions which must be satisfied at the edge of the contact region. Section 3 is devoted to the discussion on the linear stability analysis of the solutions. We show that a bifurcation occurs at a finite critical detachment length. The precise nature of the bifurcation is identified in §4: by means of a Lyapunov-Schmidt reduction of the problem, we derive the normal form of the bifurcation, and we find that the transition to a delaminated solution is generally first-order. In §5, we discuss the physical implications of our analysis. We show how the detachment length depends on the applied pressure and other model parameters such as bending stiffness and cohesive forces.

2 The model

An inextensible one–dimensional rod adheres to a straight wall. An inviscid fluid flow, ideally represented by a constant pressure normal to the rod, partially lifts the rod. We mathematically split the mechanical system into two curves in the plane: one describes the bent, non-attached portion of the rod, the other one the straight, attached part. The delaminated part is subject to a pressure p and to a vertical adhesive force that tends to restore the attached configuration. The detachment point is an unknown of the problem.

The position vector of the curve, $\mathbf{r}(s)$, is parametrised by the arclength s. We assume that the detached part of the rod spans $s \in [0, \bar{s})$, while the adhering region is $s \in [\bar{s}, +\infty]$, where $\bar{s}$ is the unknown detachment point. A unit tangent vector $\mathbf{t} = (\cos(\theta), \sin(\theta))$ is uniquely defined in every point of each curve, where $\theta(s)$ is the anticlockwise angle between the tangent vector and the x-axis. We take the unit normal as $\mathbf{n} = (\sin(\theta), -\cos(\theta))$ so that $\mathbf{t}' = -\theta' \mathbf{n}$. In the attachment point the curve is smooth: $\theta(\bar{s}) = 0$ and the tangent vector is $\mathbf{t}(\bar{s}) = \mathbf{e}_1$. By contrast, the endpoint of the non-attached portion of the rod, $s = 0$, is free.

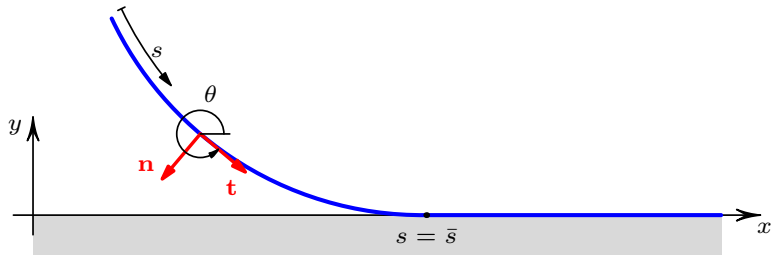

Figure 1: Schematic representation of the system geometry. The rod is parametrised by the archlength s, with origin at the free end and detachment point at $s = \bar{s}$; $\theta(s)$ is the anticlockwise angle between the tangent vector and the x-axis.

The inextensible rod stores elastic energy only because of bending

$$w(\theta', \bar{s}) = \int_0^{\bar{s}} \frac{k}{2}(\theta')^2 ds, \tag{1}$$

where k is the bending modulus and only the detached part contributes to the energy. Then, we introduce a Lagrange multiplier to account for the inextensibility constraint, and write the total energy of the rod as

$$W(\mathbf{r}, \theta, \mathbf{N}, \bar{s}) = \int_0^{\bar{s}} \Big(\frac{k}{2}(\theta')^2 - \mathbf{N} \cdot (\mathbf{r}' - \mathbf{t}) \Big) \mathrm{d}s \tag{2}$$

Here $\mathbf{N}(s) = (N_x(s), N_y(s))$ is the (unknown) reaction force in the rod due to the inextensibility constraint.

A pressure difference p and an adhesive vertical force $\mathbf{f} = f\mathbf{e}_2$ apply to the rod. The constitutive equation of the adhesive force is illustrated in the next section. We exploit the non-conservative version of the principle of virtual work, $\delta W = \delta L$, where δL is the work exerted by the non-conservative active forces

$$\delta L = \int_0^{\bar{s}} \big(-p\mathbf{n} + f\mathbf{e}_2 \big) \cdot \delta\mathbf{r} \, \mathrm{d}s, \tag{3}$$

where p is supposed to load the rod in $s \in [0, \bar{s})$, even when $y = 0$.

2.1 Equilibrium equations

The first variation of the energy functional Eq.(2) is calculated in Appendix A, and it eventually reads

$$\delta W = \int_0^{\bar{s}} \Big((-k\theta'' - N_x \sin\theta + N_y \cos\theta)\delta\theta - \delta\mathbf{N} \cdot (\mathbf{r}' - \mathbf{t}) + \mathbf{N}' \cdot \delta\mathbf{r} \Big) \mathrm{d}s - \frac{k}{2}\theta'(\bar{s})^2 \, \delta\bar{s}. \tag{4}$$

We rewrite the virtual work (3) as

$$\delta L = \int_0^{\bar{s}} \big(-p \sin\theta \, \delta x + (p\cos\theta + f)\delta y \big) \, \mathrm{d}s. \tag{5}$$

Taking into account all the possible variations, including the contact point and integrating by parts, we can calculate the Euler-Lagrange equations for this system from the principle

of virtual work, thus obtaining

$$k\,\theta'' + N_x \sin\theta - N_y \cos\theta = 0, \tag{6a}$$
$$N_x' = -p\sin\theta, \qquad N_y' = p\cos\theta + f, \tag{6b}$$
$$x' = \cos\theta, \qquad y' = \sin\theta, \tag{6c}$$

together with the following boundary conditions

$$\theta'(0) = 0, \qquad N_x(0) = 0, \qquad N_y(0) = 0, \tag{7a}$$
$$x(\bar{s}) = 0, \qquad y(\bar{s}) = 0, \qquad \theta(\bar{s}) = 0, \qquad \theta'(\bar{s}) = 0. \tag{7b}$$

Among the several possible stress-strain laws [28], we posit the following constitutive law for the adhesive force [21, 7, 26, 25]

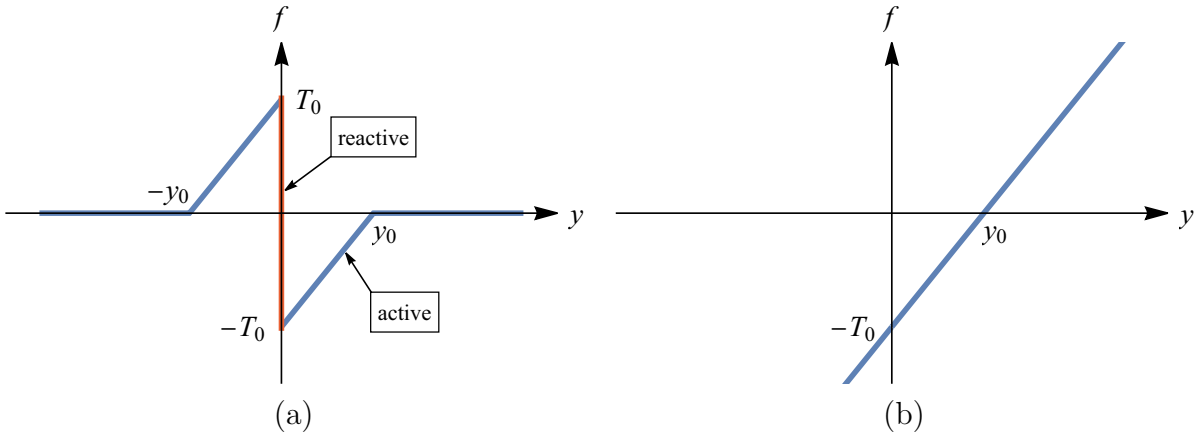

Figure 2: (a) Constitutive model for adhesion. When $y = 0$ and $|p| \le T_0$, f is a vertical reactive force that balances the pressure forces and may attain a maximum value T_0. In the active regions, $0 < y \le y_0$ or $-y_0 \le y < 0$, f decreases linearly to zero, vanishing when $y \ge y_0$ or $y \le -y_0$. (b) Regularisation of the cohesive law to be used in the local analysis of Eqs.(12) to find the onset of bifurcation about $p = T_0$, $y = 0$.

$$f = \begin{cases} -p & \text{if} \quad y = 0 \text{ and } |p| \le T_0 \quad \text{(reactive region)} \\ -T_0\big(1 - y/y_0\big) & \text{if} \quad y \in (0, y_0] \quad \text{or} \quad (y = 0 \text{ and } p > T_0) \quad \text{(active region)} \\ T_0\big(1 + y/y_0\big) & \text{if} \quad y \in [-y_0, 0) \quad \text{or} \quad (y = 0 \text{ and } p < -T_0) \quad \text{(active region)} \\ 0 & \text{otherwise} \quad \text{(active region)} \end{cases} \tag{8}$$

When $y = 0$ and $|p| \le T_0$, $\mathbf{f} = f\mathbf{e}_2$ is a reactive force that can take any suitable value to balance the external pressure. In analogy with static and dynamic friction, T_0 is the threshold force below which there is no detachment. By contrast, when $y > 0$ the adhesion is an active force whose action decreases linearly with distance according to the law as given in (8) (see Fig.2(a)). This mixed active-reactive nature of f follows from our assumption that p loads the rod in any spatial configuration, including $y(s) = 0$, in the part $s \in [0, \bar{s})$. The pressure p loads the rod in any configuration, including the straight one: a possible physical interpretation of such a law is that even if a thin layer of fluid infiltrates under the beam, co-occupying it with the the underlying glue, rod detachment

may be negligible because the adhesive forces are still able to counteract the effect of the pressure until it exceeds the critical value T_0.

The adhesion force is purely vertical, independent of the horizontal displacement and the arc parameter. This choice is consistent with a capillarity adhesion model, mediated by a fluid. Other constitutive laws are of course possible: an example is a glue represented by linear springs attached to the original location of material points [17].

For mathematical convenience, we study the "dual" problem of equations (6)-(8) in which we fix the length of the detached part, $\bar{s}$, i.e., the region where the pressure forces that tend to detach the beam act, and investigate non-trivial equilibrium solutions, and corresponding pressure values, for such $\bar{s}$. In other words, we now suppose to know $\bar{s}$, while p is unknown. To this aim, we supplement our system of equations (6) with $p' = 0$. The non-trivial solution will have $y(s) > 0$ throughout $s \in [0, \bar{s})$, while it will be $y(s) = 0$ for $s \in [\bar{s}, +\infty)$.

Since we are interested in the onset of the transition and the determination of detachment condition, we perform a local study of the solutions in a neighbourhood of $p = T_0$. Hence, it is possible to limit the analysis of cohesive forces in the active region, $y > 0$, and use a regular linear form as in Fig.2(b). This simplification implies a local validity of our analysis, so that our solutions are valid provided they lie in the range $0 \leq y \leq y_0$ and $p \geq 0$. As illustrated in Fig.3, the linearised cohesive law depicted in Fig.2(b), introduces two spurious, non-physical solutions, shown in Fig.3(c) and (e), in addition to the physically acceptable solution presented in Figure 3(a). Solution (c) must be discarded because a portion of the rod extends beyond the limit of the active region $y \leq y_0$ where a repulsive cohesive force shows up. Since our primary focus is on studying the onset of instability, where we envision y to be small, this solution does not pose a significant concern, particularly for investigating the onset of stability. The case illustrated in Fig.3(e) presents a different scenario, corresponding to a solution with $y < 0$. In this situation, the cohesive forces of the linearised constitutive law are repulsive along the entire length of the beam and have a magnitude greater than T_0.

Although this regularisation of the cohesive law may seem brutal it has the major advantage of making our problem mathematically tractable. Furthermore, it transforms it into a bifurcation problem, for which classical and powerful techniques of nonlinear analysis are available, allowing us to gain an intuitive understanding of the transition. Fake solutions introduced by the linearization, that have no meaning for the nonlinear constitutive law, will be discarded a posteriori.

It is now convenient to write the equations in non-dimensional form. To this aim, we rescale the curvilinear coordinate $s = \bar{s}\,\xi$ (so that $0 \leq \xi \leq 1$, and $\frac{d}{ds} = \frac{1}{\bar{s}}\frac{d}{d\xi}$) and introduce the following non-dimensional functions and parameters

$$\hat{\theta}(\xi) = \theta(s), \qquad \hat{N}_x(\xi) = \frac{\bar{s}^2}{k} N_x(s), \qquad \hat{N}_y(\xi) = \frac{\bar{s}^2}{k} N_y(s), \tag{9}$$

$$\hat{x}(\xi) = x(s)/\bar{s}, \qquad \hat{y}(\xi) = y(s)/\bar{s}, \qquad \alpha = \frac{\bar{s}^3 p}{k}, \tag{10}$$

$$\beta_0 = \left(\frac{\bar{s}}{\eta}\right)^3 \qquad \beta_1 = \left(\frac{\bar{s}}{\eta}\right)^3 \frac{\bar{s}}{y_0}, \tag{11}$$

where $s = \bar{s}\,\xi$ and we have introduced the *elasto-adhesion length* $\eta = (k/T_0)^{1/3}$. It is a characteristic length scale that compares the bending stiffness of the rod versus the strength of the cohesive forces [24]. The control parameter β_0 encodes the ratio between $\bar{s}$ and η, while β_1 also contains information about the decrease rate of the adhesion with height. They are independent parameters as $\bar{s}/y_0$ can be arbitrarily fixed. Hence, the

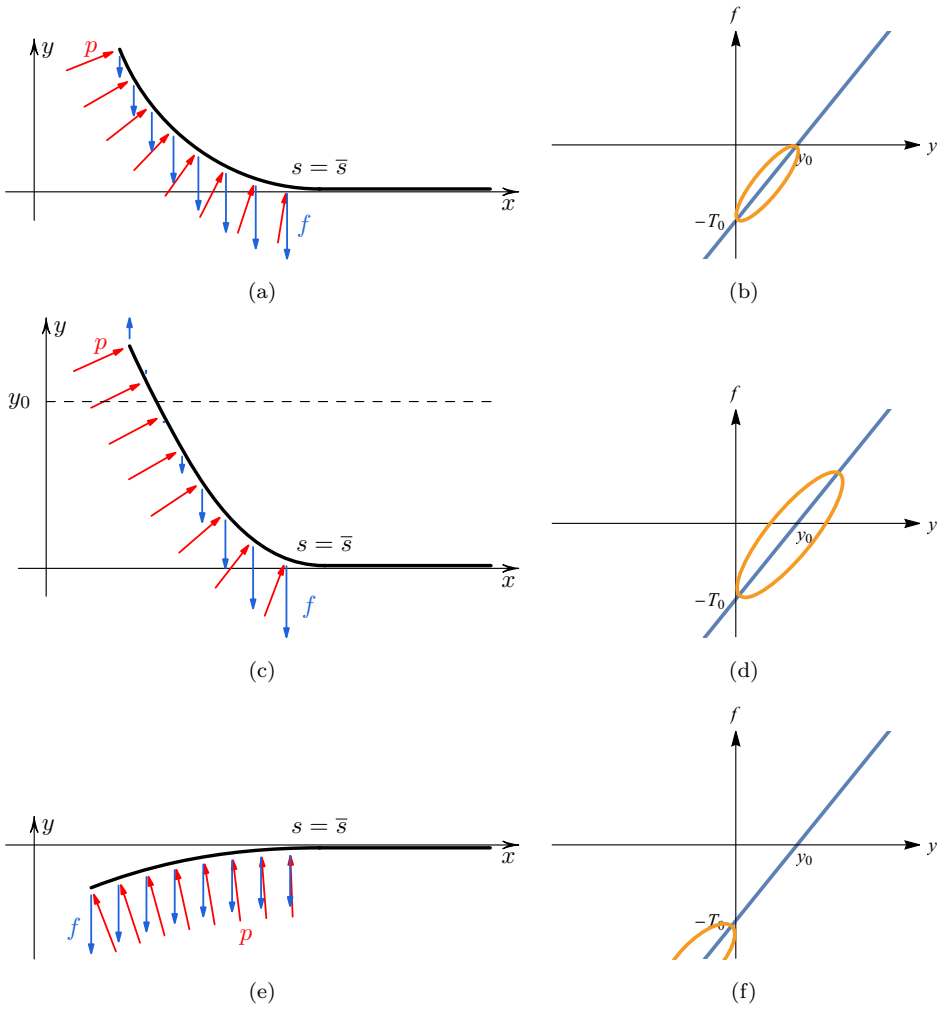

Figure 3: Profiles of possible equilibrium configurations of the rod according to the linearized adhesion law. Forces acting on the rod are indicated: pressure forces (red), which are orthogonal to the rod, and adhesive forces (blue), which are vertical. The linear simplification of the adhesive constitutive law, as shown in Fig.2(b), introduces two kind of fake solutions (c) and (e) in addition to the one acceptable for the nonlinear model too (a). These unphysical solutions must be discarded *a-posteriori*. Panels (b), (d), and (f) schematically relate the regions of the constitutive law to the corresponding adhesion forces shown in the left panels.

equilibrium equations, when the adhesion is in its active regime, read

$$\hat{\theta}'' + \hat{N}_x \sin\hat{\theta} - \hat{N}_y \cos\hat{\theta} = 0, \tag{12a}$$

$$\hat{N}_x' = -\alpha \sin\hat{\theta}, \tag{12b}$$

$$\hat{N}_y' = \alpha \cos\hat{\theta} - \beta_0 + \beta_1 \hat{y}, \tag{12c}$$

$$\hat{x}' = \cos\hat{\theta}, \qquad \hat{y}' = \sin\hat{\theta}, \tag{12d}$$

$$\alpha' = 0, \tag{12e}$$

where all fields are non-dimensional, the prime denotes derivation with respect to ξ, and physically admissible solutions have $\hat{y} \in [0, y_0/\bar{s}]$, $\beta_0 \geq 0$, and $\beta_1 > 0$. As will become clearer later, from a mathematical standpoint, it is also interesting to examine the scenario $\beta_0 = 0$. This entails adopting a linear cohesive law where $T_0 \to 0$, $y_0 \to 0$, while maintaining a constant ratio of T_0/y_0. Consequently, it involves employing a linearly *repulsive* law for f, which is not of primary interest in our physical context. Within this limit, the slope of the constitutive law, and hence that of β_1, can still be arbitrarily assigned.

We observe that $\hat{x}(\xi)$ appears only in the first equation in (12d) and it can be determined a posteriori once we know $\hat{\theta}$. The first equation in (12d) can therefore be neglected in the following analysis. We remark that we have fixed $\bar{s}$, so that the dimensionless pressure, α, is an unknown constant.

3 Linear analysis: critical detachment length

For each fixed value of $\bar{s}$, there exist an infinity of trivial solutions with $y = 0$, each one corresponding to an arbitrary pressure value $0 \leq p \leq T_0$, where the pressure forces exerted on $[0, \bar{s})$ are balanced by the adhesion forces.

We are interested in studying whether the system of equations (12) presents a bifurcation as the control parameters β_0 and β_1 vary, the attachment length $\bar{s}$ being given. By contrast, the dimensionless pressure α at equilibrium is an unknown of the problem.

Let us now focus on a neighbourhood of the limiting case $p \approx T_0$, corresponding to $\alpha = \beta_0$. There is a principal branch of solutions, i.e., a trivial solution with $\theta = 0$, $y = 0$, $N_x = 0$, $N_y = 0$ and $\alpha = \beta_0$, for every value of the parameter β_1. We want to investigate whether there are possible non-trivial equilibrium solutions which are small perturbations of $\theta = 0$, $y = 0$, $N_x = 0$, $N_y = 0$ and $\alpha = \beta_0$, for a given finite $\bar{s}$.

For notational convenience, in the following we drop the "hat" superscript for the dimensionless quantities and we linearise the equilibrium equations (12) about $\theta = 0$, $y = 0$, $N_x = 0$, $N_y = 0$ and $\alpha = \beta_0$,

$$\theta'' - N_y = 0, \tag{13a}$$

$$N_x' + \beta_0 \theta = 0, \tag{13b}$$

$$N_y' - \alpha_1 - \beta_1 y = 0, \tag{13c}$$

$$y' - \theta = 0, \tag{13d}$$

$$\alpha_1' = 0, \tag{13e}$$

where $\alpha_1 = \alpha - \beta_0$ is the unknown (constant) "extra-pressure" with respect to β_0. We remark that, given our constitutive assumption on f, only the solutions with $\alpha_1 \leq 0$ (and $y \geq 0$) are acceptable from a physical standpoint. Furthermore, the linear profile of the cohesive force is valid only until $y \leq y_0$. For mathematical convenience, however, we

consider Eq.(12c) to be valid also when $\alpha_1 > 0$, $y < 0$ or $y > y_0$, and we will discard such solutions *a-posteriori*.

The boundary conditions are

$$N_x(0) = 0, \qquad N_y(0) = 0, \qquad \theta'(0) = 0, \tag{14a}$$

$$\theta(1) = 0, \qquad \theta'(1) = 0, \qquad y(1) = 0. \tag{14b}$$

The critical condition is derived by a simple manipulation of the linear equations. After differentiation of (13a), (13c) and the substitutions obtained from (13d), (13e), we eventually get the fourth order differential equation

$$\theta^{iv} = \beta_1 \theta, \qquad (\ \beta_1 > 0\ ) \tag{15}$$

with general solution

$$\theta(\xi) = c_1\, \mathrm{e}^{\beta_1^{1/4}\xi} + c_2\, \mathrm{e}^{-\beta_1^{1/4}\xi} + c_3\, \cos(\beta_1^{1/4}\xi) + c_4\, \sin(\beta_1^{1/4}\xi). \tag{16}$$

The solution has to satisfy the boundary conditions

$$\theta'(0) = 0, \qquad \theta(1) = 0, \qquad \theta'(1) = 0, \qquad \theta''(0) = 0, \tag{17}$$

where this last boundary condition is derived from (13a), with $N_y(0) = 0$. As shown in Appendix B, non-trivial linear solutions compatible with the boundary conditions (17) can be obtained for

$$\beta_1 = (n\pi)^4, \qquad n \in \mathbb{Z} \setminus \{0\}. \tag{18}$$

We consider the first buckling mode and set $n = 1$ in the following: the critical condition becomes $\beta_1 = \pi^4$. Hence, we have found a second branch of solutions with the linear approximation of $\theta(\xi)$ expressed as

$$\theta(\xi) = A \left(\frac{\mathrm{e}^{\pi\xi} + \mathrm{e}^{\pi - \pi\xi}}{2\,(\mathrm{e}^{\pi} - 1)\,\pi^3} + \frac{\sin(\pi\xi)}{2\pi^3} + \frac{(1 + \mathrm{e}^{\pi})\cos(\pi\xi)}{2\,(\mathrm{e}^{\pi} - 1)\,\pi^3} \right), \tag{19}$$

where A is an arbitrary constant to be determined by solving the fully nonlinear problem. The presence of multiple solution branches at $\beta_1 = \pi^4$ for the linear problem is an indication of a bifurcation in the nonlinear equations (12).

In terms of the physical parameters T_0, y_0, and k, the condition $\beta_1 = \pi^4$ can be interpreted as giving a "critical detachment length". From Eq.(11), we get

$$\bar{s}_c = \pi \sqrt[4]{\eta^3 y_0} = \pi \Big(\frac{k y_0}{T_0} \Big)^{1/4}. \tag{20}$$

When $\beta_0 = 0$ the transition to a detached solution is smooth and the linear analysis provides the detachment length (20). However, as we shall see in the next section, when $\beta_0 \neq 0$, the transition turns out to be first-order (so that α_1 is discontinuous) and no conclusion can be drawn on the detachment length at the transition on the basis of the linear analysis only. Hence, in order to analyse the transition in more details and gather a more precise description of the bifurcation diagram, we need to perform a nonlinear analysis, described in the next section.

4 Lyapunov-Schmidt reduction

In an abstract setting we can rewrite Eq.(12) as $F(U,\nu)=0$ where $U=(\theta,N_x,N_y,y,\alpha_1)$, $\nu=(\beta_0,\beta_1)$ and we introduce a smooth mapping $F: X\times\mathbb{R}^2\to Y$, between Banach spaces X, Y. We can typically choose $X=C^2_0[0,1]\times(C^1_0[0,1])^4$ and $Y=(C^0_0[0,1])^5$. We recall that we use $\alpha_1=\alpha-\beta_0$ to shift the trivial solution in the origin, so that $F(0,\nu)=0$ for any value of the parameters ν. We now want to explore the possible bifurcations from the trivial solution.

A necessary condition for a bifurcation to occur at $\nu_{\rm cr}=(\beta_0,\pi^4)$ is that the linear operator L, defined as the Fréchet derivative $L:=F_U(0,\nu_{\rm cr})$, is not invertible. In our problem the linear operator L is defined by the linearized equations (13), with boundary conditions (14), when β_1 has the critical vale $\beta_1=\pi^4$. The critical condition depends only on the parameter β_1, so that strictly speaking the operator L is a function of β_0: $L=L(\beta_0)$. For ease of reading, we will omit the explicit dependence of L on β_0 in the following. Explicitly, we have

$$\begin{aligned} L\,U &= L\left(\theta,\quad N_x,\quad N_y,\quad y,\quad \alpha_1\right)\\ &= \left(\theta''-N_y,\quad N_x'+\beta_0\theta,\quad N_y'-\alpha_1-\pi^4\,y,\quad y'-\theta,\quad \alpha_1'\right), \end{aligned} \tag{21}$$

plus the boundary conditions (14) that contribute to the definition of the space X. After some algebra, we find that $K:=\ker(L)$, namely, the subspace of solutions of (13), (14) with $\beta_1=\pi^4$, is generated by $u_0=(\theta^0,N_x^0,N_y^0,y^0,\alpha_1^0)$, where

$$\theta^0(\xi)=\frac{\mathrm{e}^{\pi\xi}+\mathrm{e}^{\pi-\pi\xi}}{2\left(\mathrm{e}^{\pi}-1\right)\pi^3}+\frac{\sin(\pi\xi)}{2\pi^3}+\frac{(1+\mathrm{e}^{\pi})\cos(\pi\xi)}{2\left(\mathrm{e}^{\pi}-1\right)\pi^3} \tag{22a}$$

$$N_x^0(\xi)=\frac{\beta_0\left(-\mathrm{e}^{\pi\xi}+\mathrm{e}^{\pi-\pi\xi}+2-2\mathrm{e}^{\pi}\right)}{2\left(\mathrm{e}^{\pi}-1\right)\pi^4}-\frac{(1+\mathrm{e}^{\pi})\,\beta_0\sin(\pi\xi)}{2\left(\mathrm{e}^{\pi}-1\right)\pi^4}+\frac{\beta_0\cos(\pi\xi)}{2\pi^4} \tag{22b}$$

$$N_y^0(\xi)=-\frac{\mathrm{e}^{\pi\xi}+\mathrm{e}^{\pi-\pi\xi}}{2\pi-2\mathrm{e}^{\pi}\pi}-\frac{\sin(\pi\xi)}{2\pi}+\frac{(1+\mathrm{e}^{\pi})\cos(\pi\xi)}{2\pi-2\mathrm{e}^{\pi}\pi} \tag{22c}$$

$$y^0(\xi)=\frac{\mathrm{e}^{\pi\xi}-\mathrm{e}^{\pi-\pi\xi}+2-2\mathrm{e}^{\pi}}{2\left(\mathrm{e}^{\pi}-1\right)\pi^4}+\frac{(1+\mathrm{e}^{\pi})\sin(\pi\xi)}{2\left(\mathrm{e}^{\pi}-1\right)\pi^4}-\frac{\cos(\pi\xi)}{2\pi^4} \tag{22d}$$

$$\alpha_1^0(\xi)=1 \tag{22e}$$

In other words, the solutions of the linearised problem $LU=0$ are of the form $U=A\,u_0$, where A is an arbitrary constant. Hence, K is a one dimensional subspace of X and A determines the amplitude of the bifurcation mode (more precisely, $K_{\beta_0}\subset X$ is a family of one-dimensional vector spaces, depending on the parameter β_0). According to the normalization we chose, the arbitrary amplitude A coincides with the extra-pressure α_1.

In order to obtain a more precise picture of the bifurcation diagram, we now perform a nonlinear analysis of the bifurcation. A standard method in this context is the Lyapunov-Schmidt reduction [23, 9, 10]. This technique allows us to rewrite the problem (12), (14) as a nonlinear locally well-posed infinite dimensional one plus a finite-dimensional bifurcation equation that are easier to analyse than the original infinite-dimensional problem.

It is possible to show that L is a Fredholm operator, so that we can split the Banach spaces X and Y into the direct products $X=K\oplus K^{\perp}$ and $Y=R\oplus R^{\perp}$, where $K=\ker(L)$, $R=\mathrm{range}(L)$, $\dim(K)=1$, $\mathrm{codim}(R)<+\infty$, and we have implicitly used the L^2-scalar product $\langle\cdot,\cdot\rangle$ to define the orthogonal complements $K^{\perp}$ and $R^{\perp}$. Every $U\in X$ can be decomposed into the sum $U=u+w$, with $u\in K$ and $w\in K^{\perp}$. Likewise, our problem

$F(U,\nu)=0$ can be split into an equivalent pair of equations,

$$Q\,F(u+w,\nu)=0, \tag{23a}$$
$$(I-Q)\,F(u+w,\nu)=0, \tag{23b}$$

where Q is the orthogonal projector onto R and I is the identity. Eq.(23a), allows us to derive w as a function of u and ν (in a neighbourhood of $\nu_{\rm cr}$), while Eq.(23b), once we substitute $w=w(u,\nu)$, is a finite-dimensional equation that yields a complete, albeit local, picture of the bifurcation. Finally, we recall that, in our functional setting, it is often convenient to use the identity $R^{\perp}=\ker(L^{\dagger})$, where $L^{\dagger}$ is the adjoint operator, to calculate R and $R^{\perp}$.

The adjoint operator $L^{\dagger}:Y\to X$ is such that $\langle LU,\Phi\rangle_Y=\langle U,L^{\dagger}\Phi\rangle_X$, where $\Phi=(\phi_1,\phi_2,\phi_3,\phi_4,\phi_5)$. An explicit computation of the formal adjoint yields

$$\phi_1''+\beta_0\phi_2-\phi_4=0, \tag{24a}$$
$$-\phi_2'=0, \tag{24b}$$
$$-\phi_3'-\phi_1=0, \tag{24c}$$
$$-\phi_4'-\pi^4\phi_3=0, \tag{24d}$$
$$-\phi_5'-\phi_3=0, \tag{24e}$$

with boundary conditions $\phi_1'(0)=0$, $\phi_2(1)=0$, $\phi_3(1)=0$, $\phi_4(0)=0$, $\phi_5(0)=0$ and $\phi_5(1)=0$. From these equations we can calculate the kernel of $L^{\dagger}$ which turns out to be generated by the vector

$$\begin{aligned} v_0=\Big(&\sinh[\pi(\tfrac12-\xi)]+\sinh\left(\tfrac{\pi}{2}\right)\cos(\pi\xi)+\cosh\left(\tfrac{\pi}{2}\right)\sin(\pi\xi),0,\\ &\frac{1}{\pi}\big(\cosh[\pi(\tfrac12-\xi)]-\sinh\left(\tfrac{\pi}{2}\right)\sin(\pi\xi)+\cosh\left(\tfrac{\pi}{2}\right)\cos(\pi\xi)\big),\\ &\pi^2\big(\sinh[\pi(\tfrac12-\xi)]-\sinh\left(\tfrac{\pi}{2}\right)\cos(\pi\xi)-\cosh\left(\tfrac{\pi}{2}\right)\sin(\pi\xi)\big),\\ &\frac{1}{\pi^2}\big(\sinh[\pi(\tfrac12-\xi)]-\sinh\left(\tfrac{\pi}{2}\right)\cos(\pi\xi)-\cosh\left(\tfrac{\pi}{2}\right)\sin(\pi\xi)\big)\Big). \end{aligned} \tag{25}$$

We notice that $\ker(L^{\dagger})$ does not depend on β_0. This is evident from Eqs.(24) because from (24b) and the boundary condition $\phi_2(1)=0$, and from (24a), it follows immediately that β_0 does not enter into the calculation of $\ker(L^{\dagger})$.

We can now construct the two projectors, $P:X\to K$ and $Q:Y\to R=\ker(L^{\dagger})^{\perp}$ given explicitly by

$$Px=\langle u_0,x\rangle\,\frac{u_0}{\|u_0\|^2},\qquad x\in X, \tag{26}$$
$$Qy=y-\langle v_0,y\rangle\,\frac{v_0}{\|v_0\|^2},\qquad y\in Y. \tag{27}$$

4.1 Numerical Lyapunov-Schmidt

The analytical solution of the nonlinear problem in $w(u,\nu)$ as given in (23a), with Q as given in (27), is very cumbersome, even with the aid of a symbolic algebra system. However, as we shall see, the determination of the exact solution is not strictly necessary: we look for an approximate *numerical* Lyapunov-Schmidt reduction to identify the normal form of the bifurcation and fit the unknown coefficients to the numerical solution. To this aim, we employ the iterative method described in [2] to solve numerically (23a) and then (23b). Specifically, Eq.(23a) can be written as

$$F(u+w,\nu)-\langle v_0,F(u+w,\nu)\rangle\,\frac{v_0}{\|v_0\|^2}=0 \tag{28}$$

where $u \in K = \ker L$; $w \in K^{\perp}$; $v_0 \in \ker L^{\dagger}$. Next, we define the nonlinear (higher order) part of F as $B(u+w,\nu) := F(u+w,\nu) - L(u+w)$, where L is given as in Eq.(21). Explicitly, we find,

$$B\big((\theta, N_x, N_y, y, \alpha_1), \nu\big) = \Big(N_x \sin(\theta) + N_y(1-\cos(\theta)), \quad \beta_0(\sin(\theta)-\theta) + \alpha_1 \sin(\theta), \\ (\beta_0+\alpha_1)(1-\cos(\theta)) - \lambda y, \quad \theta - \sin(\theta), \quad 0\Big), \tag{29}$$

where we have substituted $\beta_1 = \pi^4 + \lambda$, i.e., λ measures the deviation of β_1 from the critical value $\beta_{1,\mathrm{cr}} = \pi^4$.

Since $F(u+w,\nu) = Lu + Lw + B(u+w,\nu) = Lw + B(u+w,\nu)$, and $\langle Lw, v_0\rangle = \langle w, L^{\dagger}v_0\rangle = 0$, we write (28) in the equivalent form

$$Lw + B(u+w,\nu) = \langle v_0, B(u+w,\nu)\rangle \frac{v_0}{\|v_0\|^2} \tag{30}$$

This is a convenient form for (23a) since B is a higher order remainder (i.e., it is at least quadratic in A, λ and their product) and it does not contain derivatives (see Eq.(29)). We have seen that the solutions to the linear problem are of the form $u = A\,u_0$, with u_0 as given in (22) and A an arbitrary amplitude, to be determined by the solution to the nonlinear problem. If we now fix the amplitude A, i.e., the linear solution $u = A\,u_0$, and the parameters $\nu = (\beta_0, \lambda)$, then the nonlinear correction $w(A,\nu)$ is found by solving (30). This suggests the following iterative scheme to approximate (30) [2]

$$w_0 = 0, \tag{31a}$$

$$\text{solve} \quad L\tilde{w}_{k+1} = \langle v_0, B(u+w_k,\nu)\rangle \frac{v_0}{\|v_0\|^2} - B(u+w_k,\nu), \quad (k \in \mathbb{N}) \tag{31b}$$

$$w_{k+1} = P\tilde{w}_{k+1}. \tag{31c}$$

We iterate with k until convergence. Convergence properties are discussed in [2].

Once we have obtained $w = w(A,\nu)$, we can solve the bifurcation equation (23b) to obtain the relationship between the amplitude A and the parameters β_0 and λ, thus obtaining a precise, albeit local, description of the bifurcation. In practice, we define the reduced function

$$g(A,\beta_0,\lambda) = \big\langle v_0, F\big(Au_0 + w(A,\nu);\nu\big)\big\rangle \tag{32}$$

and interpolate g over a square grid in the (λ, A) plane, for a given value of β_0. The solution to the bifurcation equation Eq.(23b) corresponds to the zero-level set $g(A,\beta_0,\lambda) = 0$.

Finally it is worth pointing out that the transversality condition for the bifurcation, as given for instance in [4, 14], is verified. In our case, this conditions requires that $F_{U\beta_1}(0,\nu_{\mathrm{cr}})[u_0] \notin R$. Since $F_{U\beta_1}(0,\nu_{\mathrm{cr}})[u_0] = (0,0,-y^0(\xi),0,0)$, the transversality condition is satisfied as $Q(0,0,-y^0(\xi),0,0) \neq (0,0,-y^0(\xi),0,0)$ as can be easily verified by direct computation.

In conclusion, the numerical Lyapunov-Schmidt reduction of our problem yields the bifurcation diagram shown in Fig.4, for $\beta_0 = 0$ and $\beta_0 = 4$, where $\lambda = \beta_1 - \pi^4$.

4.2 Analysis of the bifurcation

When $\beta_0 = 0$ we observe a supercritical pitchfork bifurcation at $\lambda = 0$, corresponding to the critical value as given in Eq.(18) (or Eq. (20)), identified in §3. However, from a physical standpoint, it is natural to require $\beta_0 > 0$. In this case (orange line in Fig. 4), a fold appears at $\lambda = \lambda_{\mathrm{F}} < 0$. This fold creates two new equilibrium solutions, not

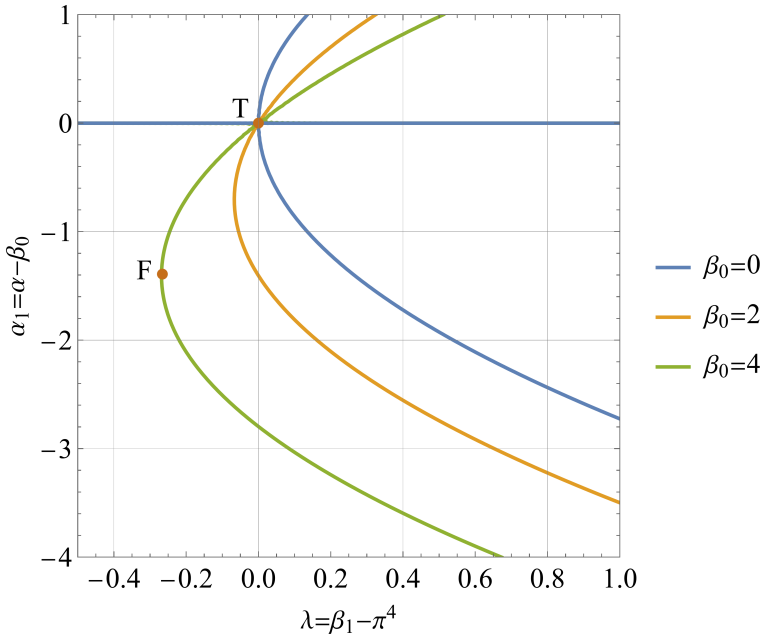

Figure 4: Bifurcation diagram obtained from the equation $g(A, \beta_0, \lambda) = 0$, for $\beta_0 = 0$ (blue line), $\beta_0 = 2$ (orange line), and $\beta_0 = 4$ (green line). We recall that the normalization constant of vector u_0 ensures its last component equals 1. Consequently, $\alpha_1 = A$ (see Eq.(22e)). The horizontal (blue) line $\alpha_1 = 0$ is the trivial solution, which exists for all values of λ and β_0.

obtainable from the linear analysis. Hence, in the range $(\lambda_F, 0)$ it is possible to observe a *discontinuous* transition to a new, detached solution, with finite detachment length and lower pressure with respect to the limit value β_0, in agreement with the numerical results in [18]. At $\lambda = 0$ (identified by point 'T' in Fig. 4) we have a transcritical bifurcation where the trivial solution becomes unstable. The different nature of the bifurcations with $\beta_0 = 0$ or $\beta_0 > 0$ can be explained by symmetry arguments. The repulsive law with $\beta_0 = 0$ is odd-symmetric with respect to the exchange $y \mapsto -y$, therefore inducing a symmetric bifurcation, namely a pitchfork. By contrast, when $\beta_0 > 0$ the symmetry is broken.

Therefore, the diagram in Fig.4 reveals that the normal form of the bifurcation is of the type

$$\alpha_1^3 + a_2\beta_0\alpha_1^2 + a_1\alpha_1\lambda = 0 \tag{33}$$

where the numerical coefficients can be found by fitting the diagram in Fig.4. We find: $a_2 \approx 0.696$ and $a_1 \approx -7.29$. Eq.(33) yields a power-law behaviour of α_1, close enough to the transition.

To validate our weakly nonlinear analysis, we numerically solve the fully nonlinear equilibrium equations (12) and find an excellent agreement between the numerical values found for the dimensionless extra-pressure α_1 and those deduced from the normal form (33), as shown in Fig.5 and in Fig.6. The direct numerical integration is obtained with the Matlab® solver `bvp4c`, by using a continuation method running backward from $\lambda \approx 1$. Equilibrium solutions of the lower and upper branches are obtained solving the full nonlinear boundary value problem starting with a guess near equilibrium, and then decreasing stepwise the value of the control parameter λ. By this simple and intuitive approach we not able to educate the algorithm to capture numerically some bifurcation branches that have been determined using the weakly nonlinear problem (no bullets in the figure 5b). More sophisticated numerical techniques would be required to this aim [11, 20].

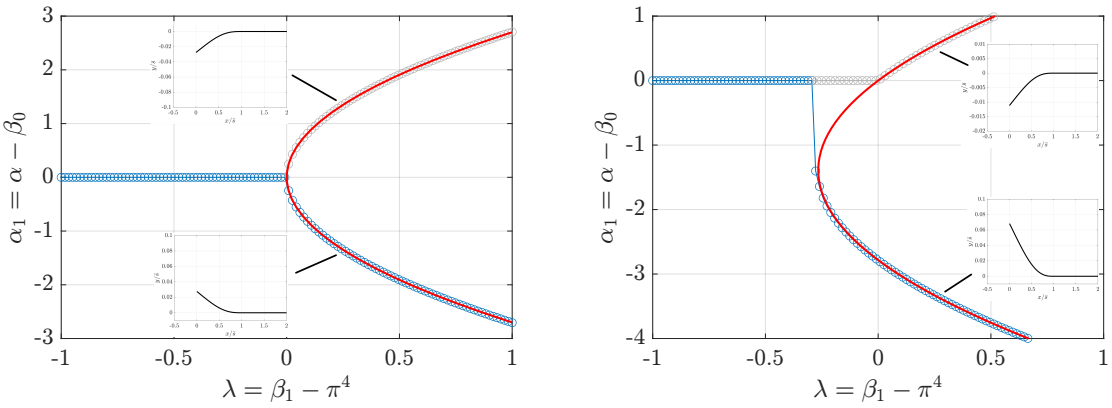

Figure 5: Dimensionless extra-pressure α_1 against λ. Gray and blue circles represent the numerical solution to the nonlinear Eqs.(12), obtained with a continuation method along the upper and lower branches, respectively, with (a) $\beta_0 = 0$ and (b) $\beta_0 = 4$. Red solid lines show the extra-pressure as obtained from the normal form Eq.(33). The numerical boundary-value problem solver, namely `bvp4c` solver in Matlab®, loses accuracy near the transition. Insets show the rod profiles with $\lambda = 0.25$.

From the normal form (33) we find that the fold F is located at

$$\lambda_{\mathrm{F}} = \frac{a_2^2\beta_0^2}{4a_1}, \qquad \alpha_{1,\mathrm{F}} = -\frac{a_2\beta_0}{2}. \tag{34}$$

An easy way to describe the key features of the bifurcation diagram is to introduce an effective potential

$$U_{\mathrm{e}}(\alpha_1;\beta_0,\lambda) = \frac{1}{4}\alpha_1^4 + \frac{1}{3}a_2\,\beta_0\,\alpha_1^3 + \frac{1}{2}a_1\,\lambda\,\alpha_1^2 \tag{35}$$

so that $\partial U_{\mathrm{e}}/\partial\alpha_1 = 0$ coincides with (33) and we are induced to study how the position and nature of the critical points of the effective potential (35) vary as far as the material parameters λ, β_0 are changed. This is shown in Fig.7 for some characteristic values of the parameters. As λ increases, the shape of the effective potential changes. The global minimum, in which the system is supposed to be, can become only a metastable local minimum and eventually vanish. More precisely, a new minimum and a new maximum appear at the fold F, corresponding to the coordinate given in (34). Physically, when $\lambda \geq \lambda_F$ the system may jump to a new, non adhering, configuration. When the actual jump occurs is the subject of two commonly applied conventions. If we adopt the *delay convention*, the transition happens when the local minimum becomes unstable. In our case, this means that the adhered solution remains until $\lambda = 0$. Another common choice is to use the so-called *Maxwell convention*: the system state is the one that globally minimizes the potential. The value at which the two minima take the same value is found by eliminating α_1 among the two equations $U_{\mathrm{e}} = 0$ and $\partial U_{\mathrm{e}}/\partial\alpha_1 = 0$, yielding

$$\lambda_M = \frac{2(a_2\beta_0)^2}{9a_1}, \qquad \alpha_{1,\mathrm{M}} = -\frac{2a_2\beta_0}{3}. \tag{36}$$

It is important to remark that the point at which the system leaves a metastable equilibrium and moves to a new equilibrium depends on the interplay between the noise level in the system and the potential barrier. It is a modelling choice that cannot be answered

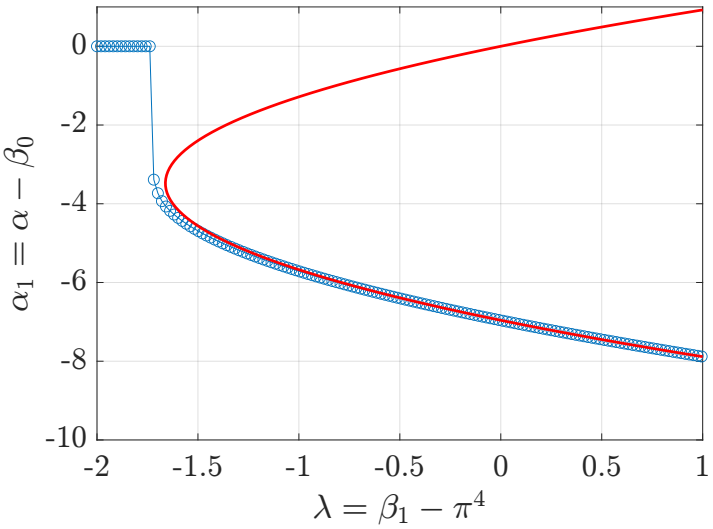

Figure 6: Like in Fig.5, but with $\beta_0 = 10$.

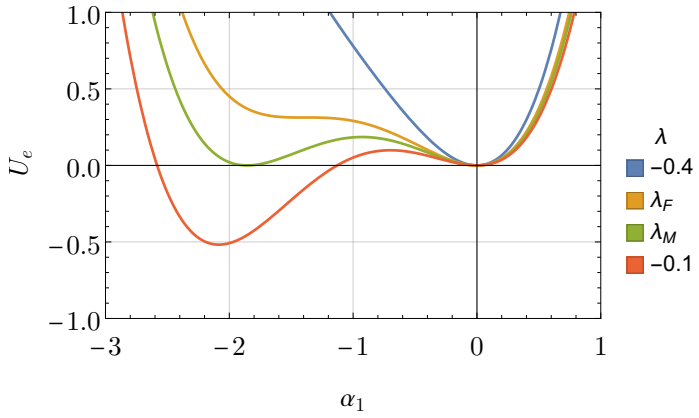

Figure 7: Effective potential, as given in (35), with $\beta_0 = 4$, for $\lambda = -0.4, \lambda_F, \lambda_M, -0.1$. When $\beta_0 = 4$, Eqs.(34),(36) yield $\lambda_F \approx -0.2658$ and $\lambda_M \approx -0.2363$.

in general, but depends on the particular physical system under study. For the sake of definitiveness, we will assume in the following discussion that the transition occurs at $\lambda = \lambda_M$ (Maxwell convention).

5 Discussion

The normal form (33) can be interpreted as an equation of state that relates the applied pressure, the detachment length and the physical characteristics of the rod and adhesive force. In order to better explore its physical significance, it is convenient to write it in dimensional form. After some algebra, Eq.(33) rewrites as

$$(p - T_0)^3 + a_2 T_0 (p - T_0)^2 + a_1 \left(\frac{\eta^3}{\bar{s}^2 y_0} - \frac{\pi^4 \eta^6}{\bar{s}^6} \right) T_0^2 (p - T_0) = 0, \tag{37}$$

where we have used the elasto-adhesion length $\eta = (k/T_0)^{1/3}$.

The lower branch of the solution, corresponding to $\alpha_1 \leq \alpha_{1,\mathrm{F}}$, is given by the equation

$$p/T_0 = 1 - \frac{a_2}{2} - \frac{a_2}{2}\sqrt{1 + \frac{4a_1}{a_2^2}\left(\frac{\pi^4\eta^6}{\bar{s}^6} - \frac{\eta^3}{\bar{s}^2 y_0}\right)} \tag{38}$$

which yields the pressure profile as a function of the detachment length $\bar{s}$, the elasto-adhesion length η and the adhesion threshold length y_0. In Fig.8 we report the pressure profile as a function of the detachment length $\bar{s}$ for various values of the ratio η/y_0. We

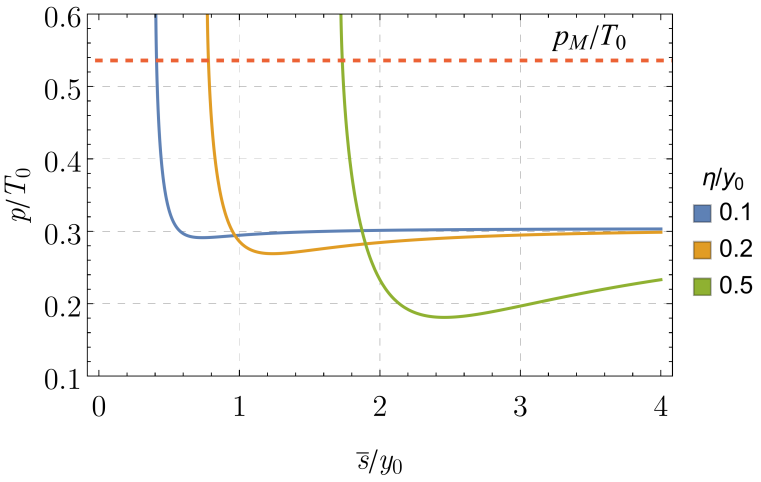

Figure 8: Pressure profile against detachment length $\bar{s}$, with $\eta/y_0 = 0.1, 0.2, 0.5, 1, 2$, as given by (38).

observe that there are in practice two different behaviours: at the transition there is a sudden drop of the applied pressure followed by a region of nearly constant pressure. To quantify this effect, we calculate the pressure at the fold F:

$$p_F = T_0\,(1 - a_2/2) \approx 0.65\,T_0, \tag{39}$$

while the pressure at the Maxwell point is found to be

$$p_M = T_0\,(1 - 2a_2/3) \approx 0.54\,T_0. \tag{40}$$

When η/y_0 is sufficiently small, the pressure, after an initial drop, is nearly constant in practice as a function of the detachment length $\bar{s}$ and tends to a value $p = p_\infty$. The limiting value of the pressure as $\bar{s}/y_0 \to +\infty$ is given by

$$p_\infty = T_0\,(1 - a_2) \approx 0.30\,T_0 \tag{41}$$

At the transition, the detachment length is finite. In other words, it is not possible to observe a delaminated solution with arbitrary small $\bar{s}$, while $\bar{s} = 0$ in the reactive region until $p \leq T_0$. This can be seen by evaluating the critical detachment length, defined as the length at the Maxwell point, which is obtained from the value of λ_M, as given in Eq.(36a). In terms of dimensional variables, we find

$$\frac{\bar{s}^4}{\eta^3 y_0} - \pi^4 = \frac{2}{9a_1}\left(\frac{a_2\bar{s}^3}{\eta^3}\right)^2 \tag{42}$$

whose solution yields the critical $\bar{s}_M$ as a function of η, shown in Fig.9. For the limited range considered in Fig.9, the critical detachment length $\bar{s}$ is well approximated by a simple linear equation $\bar{s}_M/y_0 \propto \eta/y_0$, so that $\bar{s}_M$ turns out to be largely independent of y_0 and *approximately* proportional to the elasto-adhesion length, namely, $\bar{s}_M \propto (k/T_0)^{1/3}$. This implies that a large detachment at the transition can occur for essentially two reasons: a stiffening of the rod or a deterioration of the cohesive strength. By contrast, the cohesive depth, y_0, does not seem to play a key role.

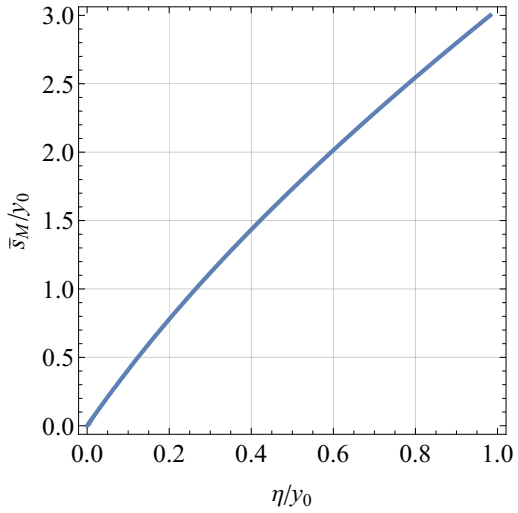

Figure 9: Detachment length at the transition (Maxwell convention), $\bar{s}_M$, as a function of the elasto-adhesion length, $\eta = (k/T_0)^{1/3}$, as deduced from (42).

Fig.8 also shows that, for some values of p, it is possible to have two equilibrium configurations with the same pressure but different detachment length and material parameters. Two paradigmatic solutions with the same pressure, are shown in Fig.10. Strictly speaking, these solutions are valid only when $y \leq y_0$, because when $y > y_0$ our analysis, that uses a linear approximation of the adhesive forces, as shown in Fig.2b, breaks down. However, when the solutions are very near to $y = y_0$, we can at least trust their qualitative features. We therefore distinguish an "unfolded" solution for small detachment lengths and a "folded" solution for large values of $\bar{s}$, where the pressure forces acting on the horizontal part do not actually tend to detach the beam but work in accordance with the adhesion forces.
Two values of $\bar{s}$, derived from Eq.(38), that correspond to the same pressure $p = 0.25\,T_0$ with $\eta = 0.566\,y_0$ are $\bar{s}^{(1)} \approx 2.128\,y_0$ and $\bar{s}^{(2)} \approx 5.664\,y_0$, corresponding, respectively, to $\beta_0^{(1)} = 53.16$, $\beta_1^{(1)} = 113.1$, and $\beta_0^{(2)} = 1001.6$, $\beta_1^{(2)} = 5670.6$. The rod shapes are shown in Fig.10. These solutions are not close to the transition, hence it is not expected that the normal form (33) (or (37)) yields accurate results. However, we obtain fairly correct values of α: Eq.(33) of our approximate analysis yield $\alpha^{(1)} = 13.29$ and $\alpha^{(2)} = 250.4$ for cases (a) and (b) of Fig.10, while the fully nonlinear numerical solution gives $\alpha^{(1)} = 14.86$ and $\alpha^{(2)} = 297.6$, respectively. We remark that the solutions are obtained using the linearised cohesive law in a range of large detachment.

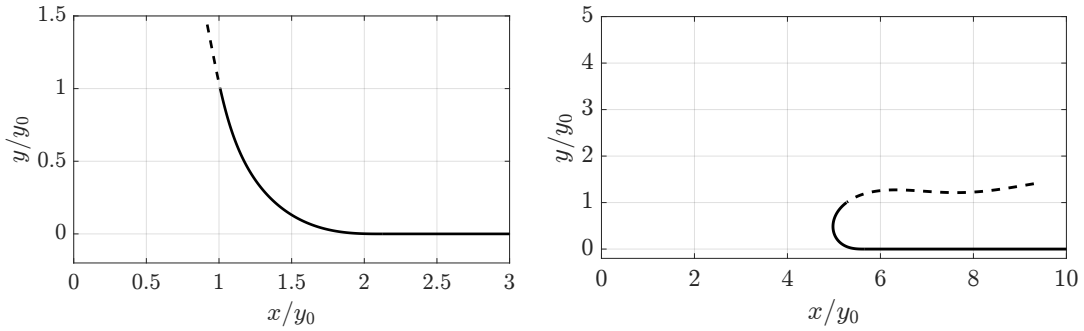

Figure 10: Rod shape for two values of $\bar{s}$ sharing the same pressure $p/T_0 = 0.25$, with $\eta/y_0 = 0.566$, as calculated from Eq.(38). (a) $\bar{s} = 2.128\, y_0$, $\beta_0 = 53.16$, $\beta_1 = 113.1$. (b) $\bar{s} = 5.664\, y_0$, $\beta_0 = 1001.6$, $\beta_1 = 5670.6$. The corresponding values of α, calculated from the normal form (33), are 13.29 and 250.4, by contrast those obtained from the numerical simulations are 14.86 and 297.6. The dashed part identifies the portion with $y(s) > y_0$, where the cohesive forces vanish, so that our simplification of a linear decreasing f, as shown in Fig.2(b), breaks down. However, in our simulations, $y(s)$ only slightly exceeds y_0 so that f is only weakly repulsive in the dashed region.

6 Conclusions

In this paper we have studied the detachment of an elastica adhering on a flat surface, induced by the lift force generated by a constant pressure difference. We rewrite the problem in terms of determination of the pressure corresponding to a given detachment length. The analysis shows that when the cohesive law is regularized and treated as an affine function across its entire range, a bifurcation occurs at a finite critical detachment length.

We first perform a linear stability analysis of the solutions and then we study the nature of the bifurcation. By means of a Lyapunov-Schmidt reduction of the problem, we derive the normal form of the bifurcation, and we find that the transition to a delaminated solution is generally first-order.

Through numerical simulations we analyze the pressure profile as a function of the detachment length for different values of the elasto-adhesion length. We observe that there are essentially two different behaviours: at the transition there is a sudden drop of the applied pressure, with a finite detachment length, followed by a region of nearly constant pressure. Therefore it is not possible to have a delaminated solution with arbitrary small $\bar{s}$, while it holds $\bar{s} = 0$ for pressures lower that T_0. Moreover it is possible to have two equilibrium configurations with the same pressure but different detachment length for some range of the control parameters. From the numerical simulations of the fully nonlinear problem we can distinguish between an "unfolded" solution (for small $\bar{s}$) and a "folded" one (for larger detachment length), where the pressure acting on the folded part works in accordance with the adhesion forces. Finally the analysis of the detachment length at the transition as a function of the elasto-adhesion length, suggests the existence of a linear relationship between the two. This indicates that a large detachment at the transition can occur for two reasons: a stiffening of the rod or a deterioration of the cohesive strength.

This paper should be considered as a first step towards understanding the lift of an elastica induced by a pressure difference. The model can be further refined in several

ways, motivating future work. For example, instead of a purely vertical adhesion force, one could consider incorporating shear resistance, introducing a horizontal component to the force. Additionally, exploring alternative constitutive models for adhesion would be beneficial. The solution obtained with a smooth nonlinear adhesion law defined in a thin layer could be studied in the limit of vanishing width, thus comparing the results with the approach discussed in this work. Furthermore, changing the geometry of the adhering surface to a more biomimetic shape, such as a circular geometry resembling an artery, could be a valuable improvement for describing phenomena like arterial dissection. Finally, investigating the effects of a pressure difference that varies along the arc length, possibly inspired by elementary solutions for fluid flow near a wall, or including skin friction drag, would be interesting avenues for future research.

Acknowledgements

This research was partially supported by GNFM of Italian Istituto Nazionale di Alta Matematica. S.T. also acknowledges the partial support by MUR, grant "Dipartimento di Eccellenza 2023-2027."

A Variational derivation

The first variation of the energy (2) is

$$\delta W = \int_0^{\bar{s}} \Big(k\theta'\delta\theta' - \delta\mathbf{N}\cdot(\mathbf{r}'-\mathbf{t}) - \mathbf{N}\cdot(\delta\mathbf{r}'-\delta\mathbf{t})\Big)\mathrm{d}s + \Big[\frac{k}{2}\theta'^2 - \mathbf{N}\cdot(\mathbf{r}'-\mathbf{t})\Big]_{s=\bar{s}}\delta\bar{s}, \quad (43)$$

where, we recall, $\mathbf{N} = N_x\mathbf{e}_1 + N_y\mathbf{e}_2$ and $\mathbf{t} = \cos\theta\,\mathbf{e}_1 + \sin\theta\,\mathbf{e}_2$. Integrating by parts and using $\delta\mathbf{t} = (-\sin\theta\,\mathbf{e}_1 + \cos\theta\,\mathbf{e}_2)\delta\theta$, we get

$$\delta W = \int_0^{\bar{s}} \Big((-k\theta'' - N_x\sin\theta + N_y\cos\theta)\delta\theta - \delta\mathbf{N}\cdot(\mathbf{r}'-\mathbf{t}) + \mathbf{N}'\cdot\delta\mathbf{r}\Big)\mathrm{d}s \quad (44)$$

$$+ \Big[\frac{k}{2}\theta'^2 - \mathbf{N}\cdot(\mathbf{r}'-\mathbf{t})\Big]_{s=\bar{s}}\delta\bar{s} + \Big[k\theta'\delta\theta - \mathbf{N}\cdot\delta\mathbf{r}\Big]_0^{\bar{s}}. \quad (45)$$

At the free end, $s = 0$, we have $N_x(0) = 0$, $N_y(0) = 0$, $\theta'(0) = 0$, therefore the second boundary term simplifies to $k\theta'(\bar{s})\delta\theta(\bar{s}) - \mathbf{N}(\bar{s})\cdot\delta\mathbf{r}(\bar{s})$. Furthermore, in the variational derivation with variable end-points [8], we need to relate $\delta\mathbf{r}(\bar{s})$, $\delta\theta(\bar{s})$ with the true variations at the end-point, namely $\delta\bar{\mathbf{r}}$ and $\delta\bar{\theta}$

$$\delta\bar{\mathbf{r}} := \mathbf{r}(\bar{s}+\delta\bar{s}) + \delta\mathbf{r}(\bar{s}+\delta\bar{s}) - \mathbf{r}(\bar{s}) \sim \mathbf{r}'(\bar{s})\delta\bar{s} + \delta\mathbf{r}(\bar{s}), \quad (46a)$$

$$\delta\bar{\theta} := \theta(\bar{s}+\delta\bar{s}) + \delta\theta(\bar{s}+\delta\bar{s}) - \theta(\bar{s}) \sim \theta'(\bar{s})\delta\bar{s} + \delta\theta(\bar{s}). \quad (46b)$$

At the detachment point, $s = \bar{s}$, we posit the Dirichlet conditions $\theta(\bar{s}) = 0$, $y(\bar{s}) = 0$. Therefore, we only consider variations of the end-point with $\delta\bar{\mathbf{r}} = \delta\bar{s}\,\mathbf{e}_1$ and $\delta\bar{\theta} = 0$. From Eq.(46) we get $\delta\mathbf{r}(\bar{s}) = \delta\bar{s}\,\mathbf{e}_1 - \mathbf{r}'(\bar{s})\delta\bar{s}$ and $\delta\theta(\bar{s}) = -\theta'(\bar{s})\delta\bar{s}$. Hence, the first variation finally reads

$$\begin{aligned}\delta W &= \int_0^{\bar{s}} \Big((-k\theta'' - N_x\sin\theta + N_y\cos\theta)\delta\theta - \delta\mathbf{N}\cdot(\mathbf{r}'-\mathbf{t}) + \mathbf{N}'\cdot\delta\mathbf{r}\Big)\mathrm{d}s \\ &+ \Big[\frac{k}{2}\theta'^2 - \mathbf{N}\cdot(\mathbf{r}'-\mathbf{t})\Big]_{s=\bar{s}}\delta\bar{s} - k\theta'(\bar{s})^2\delta\bar{s} - N_x(\bar{s})\,\delta\bar{s} + \mathbf{N}(\bar{s})\cdot\mathbf{r}'(\bar{s})\delta\bar{s} \\ &= \int_0^{\bar{s}} \Big((-k\theta'' - N_x\sin\theta + N_y\cos\theta)\delta\theta - \delta\mathbf{N}\cdot(\mathbf{r}'-\mathbf{t}) + \mathbf{N}'\cdot\delta\mathbf{r}\Big)\mathrm{d}s - \frac{k}{2}\theta'(\bar{s})^2\,\delta\bar{s}.\end{aligned} \quad (47)$$

The virtual work of the external forces is given in (3), which we rewrite as

$$\delta L = \int_0^{\bar{s}} \big(- p \sin\theta \, \delta x + (p \cos\theta + f) \delta y \big) \, \mathrm{d}s \tag{48}$$

Therefore, from the principle of virtual working, $\delta W = \delta L$, we derive Eq.(6) and the Weierstrass-Erdmann condition

$$\theta'(\bar{s})^2 = 0 \tag{49}$$

which allows us to determine the unknown detachment length $\bar{s}$, and yields the boundary condition $(7\mathrm{b})_4$. To close the problem, we get rid of the degeneracy due to the translational invariance along x by fixing the origin of the coordinate system in $s = \bar{s}$ and posit $x(\bar{s}) = 0$.

B Critical condition

When we insert the solution (16) into the boundary conditions (17), we obtain a system of linear equations in the unknowns c_1, c_2, c_3, and c_4 with associated coefficient matrix

$$A = \begin{pmatrix} \gamma & -\gamma & 0 & \gamma \\ \mathrm{e}^{\gamma} & \mathrm{e}^{-\gamma} & \cos(\gamma) & \sin(\gamma) \\ \mathrm{e}^{\gamma}\gamma & -\mathrm{e}^{-\gamma}\gamma & -\gamma\sin(\gamma) & \gamma\cos(\gamma) \\ \gamma^2 & \gamma^2 & -\gamma^2 & 0 \end{pmatrix}, \tag{50}$$

with $\gamma = \beta_1^{1/4}$. The determinant of A is,

$$\det(A) = -4\gamma^4 \sin(\gamma)\sinh(\gamma). \tag{51}$$

Hence, a non-zero solution is found when $\det(A) = 0$, from which we derive the critical condition (18).

References

[1] Eduard Arzt, Stanislav Gorb, and Ralph Spolenak. From micro to nano contacts in biological attachment devices. *Proceedings of the National Academy of Sciences*, 100(19):10603–10606, 2003.

[2] Peter Ashwin, Klaus Böhmer, and Zhen Mei. A numerical Liapunov-Schmidt method with applications to Hopf bifurcation on a square. *Mathematics of Computation*, 64(210):649–670, 1995.

[3] Siegfried Bauer, Simona Bauer-Gogonea, Ingrid Graz, Martin Kaltenbrunner, Christoph Keplinger, and Reinhard Schwödiauer. 25th anniversary article: A soft future: From robots and sensor skin to energy harvesters. *Advanced Materials*, 26(1):149–162, 2014.

[4] Michael G Crandall and Paul H Rabinowitz. Bifurcation from simple eigenvalues. *Journal of Functional Analysis*, 8(2):321–340, 1971.

[5] Hans Dannenberg. Measurement of adhesion by a blister method. *Journal of Applied Polymer Science*, 5(14):125–134, 1961.

[6] Jerald L Ericksen. *Introduction to the Thermodynamics of Solids*. Springer, New York, NY, 1998.

[7] A Ferrara and Anna Pandolfi. A numerical study of arterial media dissection processes. *International Journal of Fracture*, 166:21–33, 2010.

[8] I.M. Gelfand and S. V. Fomin. *Calculus of Variations*. Prentice-Hall, New Jersey, 1963.

[9] Martin Golubitsky and David G. Schaeffer. *Singularities and Groups in Bifurcation Theory: Volume I*. Applied Mathematical Sciences. Springer, New York, NY, 1985.

[10] Martin Golubitsky and Ian Stewart. *The symmetry perspective: from equilibrium to chaos in phase space and physical space*, volume 200. Springer Science & Business Media, 2003.

[11] Timothy J Healey. A group-theoretic approach to computational bifurcation problems with symmetry. *Computer Methods in Applied Mechanics and Engineering*, 67(3):257–295, 1988.

[12] K Kendall. The adhesion and surface energy of elastic solids. *Journal of Physics D: Applied Physics*, 4(8):1186, 1971.

[13] K Kendall. Thin-film peeling-the elastic term. *Journal of Physics D: Applied Physics*, 8(13):1449, sep 1975.

[14] Hansjörg Kielhöfer. *Bifurcation Theory*. Springer New York, NY, 2 edition, 2012.

[15] Dae-Hyeong Kim, Nanshu Lu, Rui Ma, Yun-Soung Kim, Rak-Hwan Kim, Shuodao Wang, Jian Wu, Sang Min Won, Hu Tao, Ahmad Islam, Ki Jun Yu, Tae il Kim, Raeed Chowdhury, Ming Ying, Lizhi Xu, Ming Li, Hyun-Joong Chung, Hohyun Keum, Martin McCormick, Ping Liu, Yong-Wei Zhang, Fiorenzo G. Omenetto, Yonggang Huang, Todd Coleman, and John A. Rogers. Epidermal electronics. *Science*, 333(6044):838–843, 2011.

[16] Daniel Maugis. *Contact, adhesion and rupture of elastic solids*, volume 130. Springer, 2000.

[17] D E Moulton, T H Lessinnes, and A Goriely. Morphoelastic rods. part I: A single growing elastic rod. *Journal of the Mechanics and Physics of Solids*, 61(2):398–427, 2013.

[18] G Napoli and A Goriely. A tale of two nested elastic rings. *Proceedings of the Royal Society A: Mathematical, Physical and Engineering Sciences*, 473(2204):20170340, 2017.

[19] Oliver M. O'Reilly. *Modeling Nonlinear Problems in the Mechanics of Strings and Rods*. Springer, New York, NY, 2017.

[20] Shrinidhi S Pandurangi, Ryan S Elliott, Timothy J Healey, and Nicolas Triantafyllidis. Stable spatially localized configurations in a simple structure—a global symmetry-breaking approach. *Journal of Elasticity*, 142:163–199, 2020.

[21] Raymond H. Plaut, Nurocha L. Williams, and David A. Dillard. Elastic analysis of the loop tack test for pressure sensitive adhesives. *The Journal of Adhesion*, 76(1):37–53, 2001.

[22] Paolo Podio-Guidugli. Peeling tapes. In Paul Steinmann and Gérard A. Maugin, editors, *Mechanics of Material Forces*, pages 253–260, Boston, MA, 2005. Springer.

[23] H. Rand Richard and Dieter Armbruster. Perturbation methods, bifurcation theory and computer algebra. *Applied Mathematical Sciences*, 1987.

[24] Benoit Roman and José Bico. Elasto-capillarity: deforming an elastic structure with a liquid droplet. *Journal of Physics: Condensed Matter*, 22(49):493101, 2010.

[25] Lei Wang, Nicholas A Hill, Steven M Roper, and Xiaoyu Luo. Modelling peeling-and pressure-driven propagation of arterial dissection. *Journal of Engineering Mathematics*, 109:227–238, 2018.

[26] Lei Wang, Steven M Roper, Nicholas A Hill, and Xiaoyu Luo. Propagation of dissection in a residually-stressed artery model. *Biomechanics and Modeling in Mechanobiology*, 16(1):139–149, 2017.

[27] JG Williams. Energy release rates for the peeling of flexible membranes and the analysis of blister tests. *International Journal of Fracture*, 87:265–288, 1997.

[28] HB Yin, LH Liang, YG Wei, ZL Peng, and SH Chen. Determination of the interface properties in an elastic film/substrate system. *International Journal of Solids and Structures*, 191:473–485, 2020.

[29] Hyunwoo Yuk, Teng Zhang, Shaoting Lin, German Alberto Parada, and Xuanhe Zhao. Tough bonding of hydrogels to diverse non-porous surfaces. *Nature materials*, 15(2):190–196, 2016.

[30] Hyunwoo Yuk, Teng Zhang, German Alberto Parada, Xinyue Liu, and Xuanhe Zhao. Skin-inspired hydrogel–elastomer hybrids with robust interfaces and functional microstructures. *Nature communications*, 7(1):12028, 2016.